

DEEP SPECTROSCOPY UNDER HIGH SPATIAL RESOLUTION OF THE HIGH-REDSHIFT RADIO SOURCE 3CR 368: THE MONSTER ELUCIDATED

F. HAMMER¹

DAEC, Observatoire de Paris-Meudon, 92195 Meudon Principal Cedex, France

O. LE FÈVRE^{1,2}

Canada-France-Hawaii Telescope Corporation, P.O. Box 1597, Kamuela, HI 96743

AND

D. PROUST¹

DAEC, Observatoire de Paris-Meudon, 92195 Meudon Principal Cedex, France

Received 1990 June 18; accepted 1990 December 5

ABSTRACT

New spectroscopic measurements of 3CR 368 under unmatched spatial resolution are presented. 3CR 368 had been previously widely studied at all frequencies and had been taken as an “archetype” of the high- z radio galaxies. However, we found that the brightest optical component of 3CR 368 is a foreground object and is likely to be a Galactic star—possibly a M5 dwarf—rather than a foreground galaxy. Removing the foreground object decreases the 3CR 368 luminosity substantially especially at red and infrared wavelengths. The spectral energy distribution of the 3CR 368 optical counterpart is also substantially modified. It may also alter the radio properties and the previously reported optical polarization. The residual source at $z = 1.13$ actually shows very strong and somewhat broad emission lines associated with a flat and slightly reddened continuum. 3CR 368 therefore resembles more an AGN associated with an extended emission-line region rather than a distant galaxy dominated by stellar emission. This result emphasizes the danger in interpreting such peculiar and rare distant radio sources as multiple-component high-redshift galaxies without paying attention to the possible contamination by foreground objects, such as Galactic stars or faint galaxies.

Subject headings: galaxies: redshifts — radio sources: galaxies — radio sources: identifications

1. INTRODUCTION

Since the beginning of the 1980s, identifications of faint optical counterparts of radio sources have provided several tens of distant objects which do not appear compact like radio-loud QSOs, present relatively narrow emission lines and extended emission, and are called radio galaxies. The identification of steep radio spectrum sources have allowed observers to reach redshift records comparable to these of QSOs (0902+34, $z = 3.4$, Lilly 1988; and probably 4C 41.17, $z = 3.8$, Chambers, Miley, & van Breugel 1990). One of the main questions arising about these objects is to what extent they could be considered as galaxies and then compared to less distant and better known radio galaxies or even bright ellipticals. Their apparently extended optical morphologies added to their small dispersion in a K ($2.2 \mu\text{m}$)- z relation (see, e.g., Lilly 1990) is believed to favor a stellar origin for their continuum emission. On the other hand, the discovery that quite a large fraction of them show alignments between their optical and radio axis (McCarthy et al. 1987; Chambers et al. 1987) suggests a link between radio and optical activity and leaves the door open for a nonstellar emission scenario. Infrared imaging and photometry would be helpful to tackle the issue and is still underway (Lilly 1988; Chambers, Miley, & Joyce 1988; Eisenhardt & Chokshi 1990; Djorgovski et al. 1990). However, several facts could alter our view of such distant faint objects and complicate any scenario built for them.

First, cosmological redshifts imply large surface brightness dimming and a need for high spatial resolution, because at $z = 1$, even a giant elliptical could be unresolved under $1''$ FWHM (see, e.g., Hammer 1989). The K - z relationship could be altered since it was obtained through very large apertures, several times the source sizes, and true two-dimensional photometry is needed to define better this relationship. The alignments are also dependent on the choice of the limiting surface brightness and can prove to be different when high spatial resolution two-dimensional maps are available. We (Le Fèvre et al. 1988b; Le Fèvre, Hammer, & Jones 1988a; Le Fèvre & Hammer 1988; Hammer & Le Fèvre 1990) have spatially resolved under ~ 0.8 FWHM most of the morphologies of the high- z 3CR galaxies which constitute the main part of the $z \geq 1$ radio galaxies. Typically a high- z 3CR galaxy consists of several components which often show striking differences in their spectral energy distribution from ultraviolet to infrared (see, e.g., Hammer 1989).

Second, one has to be aware of the selection criterion used to isolate these sources, especially because they have a very low density, i.e., less than one per $(1000 \text{ Mpc})^3$. It is unlikely that such peculiar sources could be the parent population of elliptical galaxies at low- z . The high- z 3CR sources all have radio fluxes very close to the catalog flux limit and it could be provided either by their strong intrinsic radio power—which suggests strong nuclear activity—and/or by complex selection effect processes. The later were suggested by Hammer, Nottale, & Le Fèvre (1986): gravitational magnification of light by foreground galaxies and clusters could help less powerful sources—which belong to a more normal population—to enter the 3CR catalog. More recently, we have given statistical evi-

¹ Visiting Astronomer, Canada-France-Hawaii Telescope, operated by the National Research Council of Canada, The Centre National de la Recherche Scientifique of France, and the University of Hawaii; partly based on observations collected at the European Southern Observatory, La Silla, Chile.

² Also Paris-Meudon Observatory.

dences of an excess of foreground bright galaxies and clusters around the sources lines of sight and outlined that at least five sources among the 27 studied were actually gravitationally magnified (Hammer & Le Fèvre 1990).

We think that most of the questions about the nature of the high- z radio galaxies are still unanswered. Their emission could be dominated by either stellar or nuclear emission. They could be affected by complex and strong selection effects and/or they could form a heterogeneous population. Their complex morphologies may be the signature of intrinsic radio/optical activity or also the blend with foreground objects of various origins—unrelated stars and galaxies, projected cluster galaxies. Then it is not without danger to derive a single scenario from the global properties of these sources. It is crucial to obtain high spatial resolution deep spectroscopy and imagery, not only globally but for each component revealed within a single high-redshift object, in order to isolate their properties, i.e., the individual nature of their components. Recently we have spectroscopically identified the two components of 3CR 208.1 and found that the faintest one was a foreground Seyfert galaxy which gravitationally magnifies the background radio-loud QSO enough to imply a removing of this source from the 3CR catalog (Le Fèvre & Hammer 1990). We present here new spectroscopic measurements of 3CR 368, for which we also find contamination by a foreground object. This source has been taken by several authors as an “archetype” of the high- z 3CR galaxies from its luminosity, its colors, its morphology, and the alignment between radio and optical axis and has been the object of numerous studies (Djorgovski et al. 1987; Chambers et al. 1988; di Seregho Alighieri et al. 1989; Chambers & Charlot 1990; Scarrott et al. 1990b; Djorgovski et al. 1990). We will show here that 3CR 368 well deserves the name of monster that one of us (F. H.) called it during an (active) discussion at a seminar given by S. Djorgovski in Paris in 1986. These new observations should bring some modesty to all people involved in this field—including us—since the foreground contamination appears more foreground than we ever believed before and deeply modifies the observed properties of the real $z = 1.13$ object.

2. OBSERVATIONS

The observations were conducted in two runs which led to two distinct sets of data. The first run was at the Canada-France-Hawaii 3.6 m telescope in 1989 July; we used the focal reducer, the V150 grism, a Ford CCD with 516×516 pixels of $20 \mu\text{m}$ and $7.5e^-$ readout noise, and a $\sim 2''$ slit. This gave a spatial resolution of $0''.4 \text{ pixel}^{-1}$, a usable spectral range from 4850 to 9200 Å, and a spectral resolution of 38 Å as measured on calibration lamp spectra, and verified on strong night sky emission lines. Three exposures, of 45 minutes each, were obtained under good seeing conditions measured to be $\sim 0''.8$ FWHM on images taken before the spectroscopic exposures. The slit position was at P.A. = $21^\circ.5$ and is indicated on Figure 1. We took special care to shift the location of 3C 368 on the slit by $\sim 10''$ between each exposure, so that the individual spectra cannot be affected by the same area of the CCD. This procedure later ensures that, after proper shift and add techniques, the final spectrum is not affected by any CCD defect. The data were later processed using standard long-slit procedures within the NOAO/IRAF data reduction package, and the spectra were flux-calibrated using the standard star Kopff 27 (Stone 1977). We used the “background” routine in the IRAF/long-slit package to correct for the sky background: we

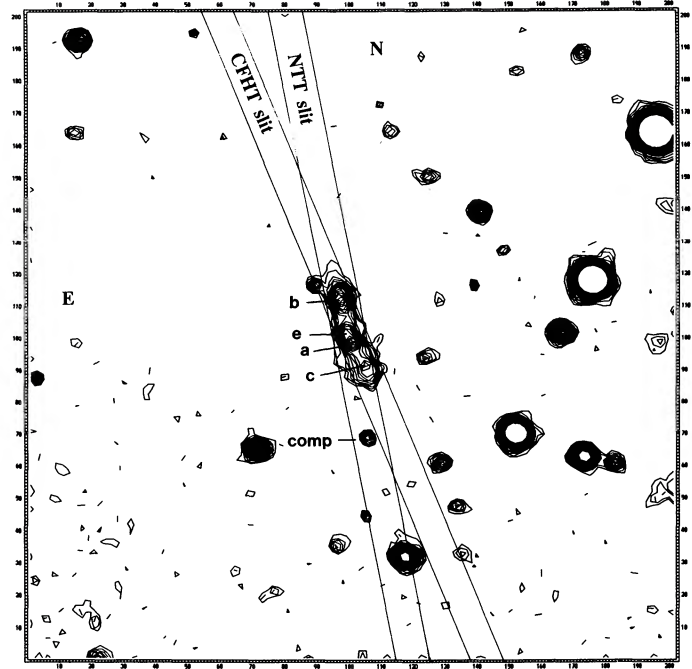


FIG. 1.—2400 s B image of 3CR 368, FWHM = $0''.75$. The field is $20 \times 20 \text{ arcsec}^2$, and the slit positions for the CFHT and NTT as well as the location of the individual components discussed in the text are indicated.

fitted a fifth-order cubic spline to each of the CCD rows, averaged over eight individual pixels, perpendicular to dispersion, and excluding from the fit the CCD region containing the spectrum of 3C 368 ($\sim 10''$ along the slit). The spline curves, including the location of 3C 368, were then subtracted to the data for each CCD row. The corrected spectra were then registered and co-added using a sigma-clipping algorithm to get rid of the cosmic ray events. Note that the calibration data on Kopff 27 does not go beyond 8400 Å, and we were not able to observe other standard stars to extend the flux calibration over our full wavelength range. In order to get a crude estimate of the relative flux between 8400 and 9200 Å, we used a simple extrapolation from the Kopff 27 flux distribution between 7500 and 8400 Å. This flux calibration was later refined using the data from our second run, better calibrated up to 8500 Å.

The second observing run was with the ESO 3.5 m NTT in 1990 February. We used the EFOSC2 instrument with the R150 grism, a Thomson CCD with 1024×1024 pixels of $19 \mu\text{m}$, and $8e^-$ readout noise, binned 2×4 , and a $2''.2$ slit at P.A. = 10° (Fig. 1). This gave a spatial resolution of $0''.33 \text{ pixel}^{-1}$, a usable spectral range from 5850 to 8500 Å, and a spectral resolution of 41 Å as measured on calibration lamp spectra and verified on strong night sky emission lines. Three exposures of 45, 50, and 50 minutes, were obtained under seeing conditions around $0''.9$ FWHM as measured on images taken before each spectroscopic exposure. Again, we used the same shift and add technique to avoid any CCD systematics. The data were flux-calibrated using the stars LTT 2415 and LTT 4816 (Stone & Baldwin 1983). The calibrated two-dimensional spectra were then registered and co-added using a sigma-clipping algorithm to get rid of the cosmic-ray events.

The resulting total CFHT spectra for each of the four main

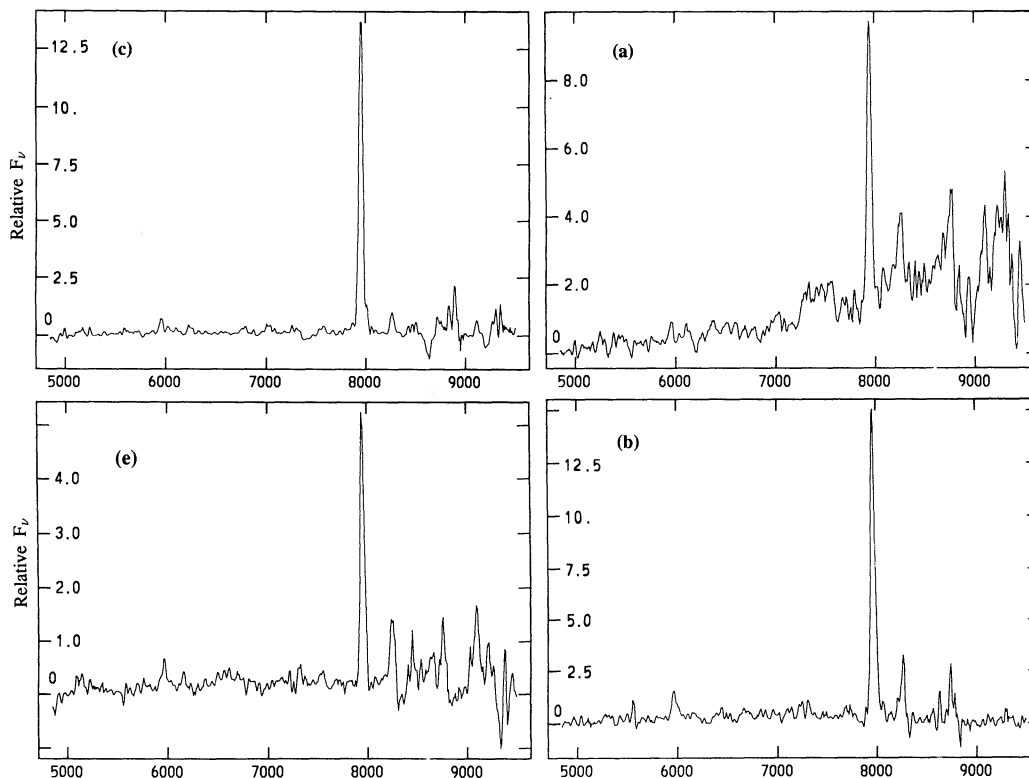


FIG. 2.—CFHT spectra of the individual components (a), (b), (c), and (e)

components are presented in Figure 2. The reader is referred to the *B* band image of Le Fèvre et al. (1988a), for the definition of components (a)–(d); we define here the resolved intensity peak detected in the *B*-band $0''.75$ north of component (a) as component (e) (see also Fig. 1). A careful signal-to-noise ratio evaluation has been made in order to set the level of details that one should consider for interpretation. Figure 3 displays the total NTT spectrum of component (a) and the associated residual noise at any given wavelength both extracted from the final two-dimensional spectrum obtained after the data processing (consisting of bias and flat-field corrections, sky emission subtraction, extinction correction, and flux calibration for each individual spectrum which were then registered and averaged using a sigma-clipping algorithm). The “noise” spectrum on Figure 3 has been produced by plotting 10 spectra extracted on the final processed two-dimensional CCD spectrum $\pm 30''$ along the slit on each side of 3C 368, in regions devoid of objects, and with the same extraction profile as was used for component (a). These spectra therefore give an accurate representation of the residual noise one can expect on the component (a) spectra after the data processing; *S/N* values on critical regions of the spectra are indicated in Figure 3. Note that our data processing provides an excellent sky subtraction over the observed wavelength range. The average sky-corrected flux per pixel is $0 \pm 2\%$ – 3% of the sky emission for the strongest sky lines like $O\ I\ 5577\ \text{\AA}$, $O\ I\ 6300\ \text{\AA}$ and $0 \pm 1\%$ over a typical OH sky band, and is very stable along the whole slit (3.5 at the CFHT, 2.8 at the NTT) with extreme local residuals $\leq 2\%$ of the sky brightness along a full CCD row (fixed wavelength). We choose to present here spectra not corrected for atmospheric absorption features to avoid introducing extra noise in the data. However, we did use, when

necessary, slightly noisier spectra corrected for atmospheric absorption features extracted from standard star spectra.

3. SPECTROSCOPIC NATURE OF INDIVIDUAL COMPONENTS

During our two observing runs, both seeing conditions and long exposure times have provided us unmatched data on this source. Separations between the four components (a, b, c, and e) along the slit are between $0''.75$ and $1''.5$ while the seeing

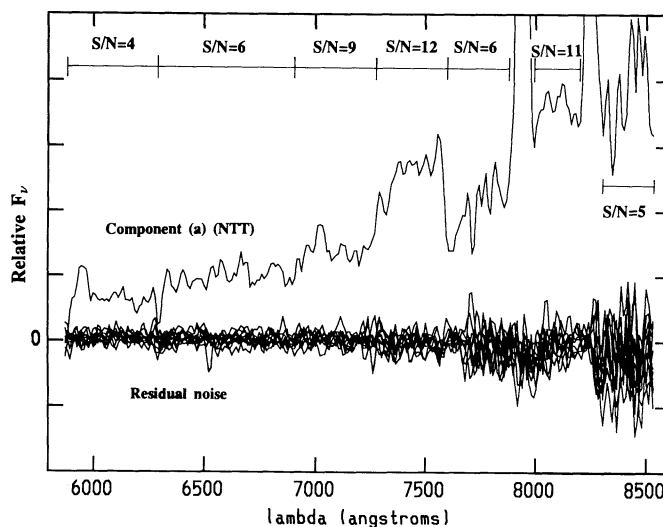


FIG. 3.—Final spectrum of (a) from the NTT observations and its associated residual noise; both were extracted from the final processed NTT spectrum (see text).

FWHM were between $0''.8$ and $1''.0$. We therefore are able to present here spectroscopy of individual components of the optical source which lies between the two radio components of 3CR 368. Our previous imaging (Le Fèvre et al. 1988a) made us aware of a probable spectral contamination of a component by its neighbor, since (e) is blended with (a) in the R frame, and (c) seems sufficiently extended to contaminate (a) spectroscopically. Our spectroscopic results have definitively confirmed the essentially different natures of the optical components in 3CR 368 since (1) component (a) has a strong and red continuum; (2) components (c) and (e) are dominated by strong emission lines with no or extremely faint continua;

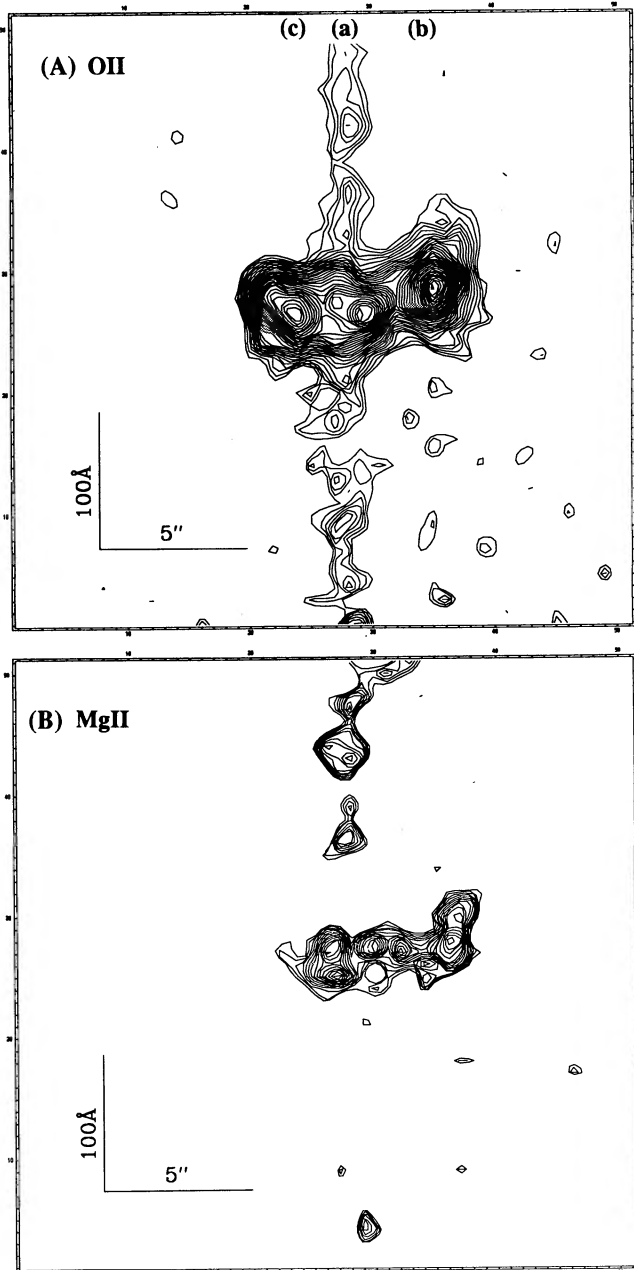


FIG. 4.—Two-dimensional spectra $21'' \times 450 \text{ \AA}$ enlargements (a) centered on the $[\text{O II}] \lambda = 3727$ line redshifted to $\lambda = 7950 \text{ \AA}$; (b) centered on the $[\text{Mg II}] \lambda = 2799$ line redshifted to $\lambda = 5970 \text{ \AA}$.

TABLE 1
EMISSION-LINE SPECTROSCOPIC DATA

Parameter	Mg II 2799	Ne V 3426	O II 3272	Ne III 3869
Component (a)				
FWHM (\AA)	38.0	38.4
Relative flux	2.5	...	40.9	9.9
Component (b)				
Equivalent width (\AA)	160	(54)	846	494
FWHM (\AA)	36.5	18.7	29.9	...
Relative flux	8.8	(3)	73.1	10.9
Component (c)				
FWHM (\AA)	30.4	32.4
Relative flux	2.5	...	69.2	3.4
Component (e)				
FWHM (\AA)	...	25.1	29.6	41.0
Relative flux	2.8	1.5	24	5.9

and (3) component (b) has a faint continuum with a strong emission-line system redshifted by $\sim 550 \text{ km s}^{-1}$ from the other components. The Figure 4 show the spatial differences seen along the slit for the $[\text{O II}] 3727 \text{ \AA}$ and $[\text{Mg II}] 2799 \text{ \AA}$ lines, and Table 1 summarizes the emission-line properties for each component.

3.1. Spectra of the "Red" Central Component (a) and of a Faint Companion $6''.3$ South of (a)

Even before our spectroscopic work, our attention was focused on component (a), since it presented discrepant colors relative to the other components (Le Fèvre et al. 1988a). Strong emission lines are also detected in its spectrum—including $[\text{O II}] \lambda 3727 \text{ \AA}$ —all of which being identified with the redshift system at $z = 1.13$. One should note that the emission line profiles along the slit strikingly show a minimum at (a) and maxima on both sides of (a), i.e., on (c) and (e) while the continuum has a pronounced peak on (a) (Fig. 5a). Component (a) is the place of a strong and sharp minimum of the equivalent widths of all the emission lines which was already visible on the Figure 6 of Djorgovski et al. (1987). This strongly suggests that the emission lines detected on component (a) spectrum are emitted from a distinct region relative to the red continuum described below. Indeed, we have found that these emission lines are likely to be due to the spatial contamination by the (e) emission-line spectrum since this component lies at $0''.75$ from (a) as well as contamination by the (c) emission line spectrum since (c) appears very spatially extended toward component (a). Simple Gaussians were fitted on the O II emission line at the (c) and (e) locations and then co-added and their contributions at the location of (a) were found to be roughly equal to the intensity measured on the data. The velocity distribution in the $[\text{O II}] \lambda 3727$ along the slit is consistent with this hypothesis since there is only a marginal discrepancy—about $200 (\pm 50) \text{ km s}^{-1}$ —between the velocity of (a) and those of (c) and (e) (Fig. 5b). This discrepancy seems to be the signature of intrinsic velocity dispersions inside (c) and (e) because both (c) and (e) velocities decrease toward component (a). In the following, we will assume that the emission lines are not intrinsic features of component (a), and their contamination origin will be confirmed by several independent arguments.

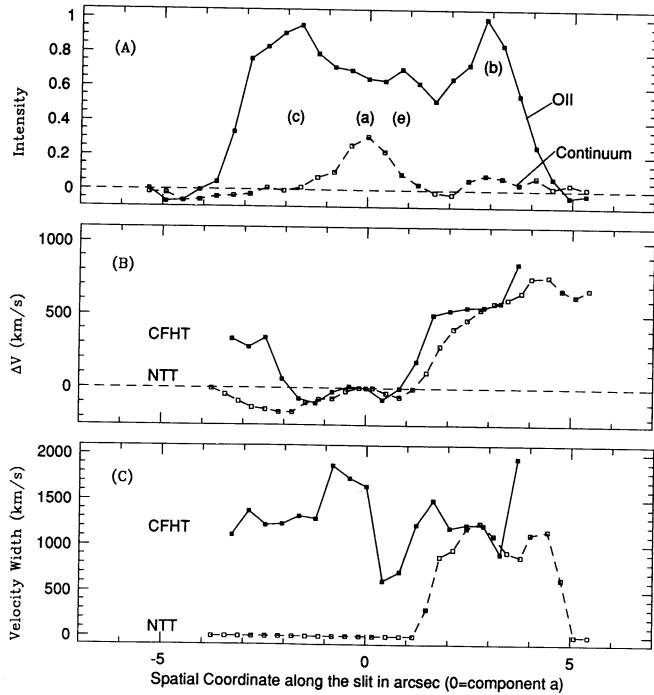


FIG. 5.—(a) Continuum intensity distribution (dashed line) and [O II] emission-line spatial intensity distribution along the CFHT slit, after removal of the continuum emission (solid line). (b) Spatial distribution of [O II] line radial velocity along the slit for the CFHT data (solid) and the NTT data (dashed). (c) [O II] Velocity width spatial distribution along the CFHT slit (solid) and NTT (dashed).

We then focus our attention on the “red” continuum which is probably the only important spectral signature of component (a). The highest significant features—i.e., with a S/N well above 5—are provided by the spectral energy distribution (SED) of the continuum (Fig. 3). The later is dominated by a huge “break” around 7300 \AA with an increase of the flux by more than a factor of 2 from $\lambda \leq 7250 \text{ \AA}$ to $\lambda \geq 7350 \text{ \AA}$, with another increase of the flux redward of 8000 \AA : 1.5 time more flux above 8000 \AA than below 7850 \AA . A careful examination of the spectrum of the whole optical source obtained by Djorgovski et al. (1987) also shows these features as well as an individual spectrum of (a) taken by A. Stockton (private communication), although with a lesser S/N . The blue part of the continuum below 7000 \AA shows a smooth decrease of the energy distribution down to 5000 \AA —and even 4000 \AA as indicated by the $B-R$ color index of (a). The red part of the continuum still shows a typical S/N of 10 (see Fig. 3) with most of the noise being the residual of the night sky OH bands subtraction. Another indication on the nature of the component (a) SED is given by a faint object—hereafter called companion—lying at $6''.3$ S of component (a) (see Fig. 1), and which has a comparable $B-R$ color index. We have included it into the slit during our observing run at the ESO NTT and despite of its faintness $R = 22.2 \pm 0.07$, the spectrum of the companion between 5900 and 8500 \AA (see Fig. 6) reveals a significant “break” at 7400 \AA with a factor of 2.5 increase of the flux ($S/N = 4$), as well as a significant increase of the flux redward of 8000 \AA by a factor 1.5 ($S/N = 3.5$). There is also a feature at 7030 \AA similar to the one found in component (a) spectrum ($S/N = 2$). The companion spectrum therefore strongly resembles the SED of the component (a) continuum! Since the companion has no emission line, this strongly sup-

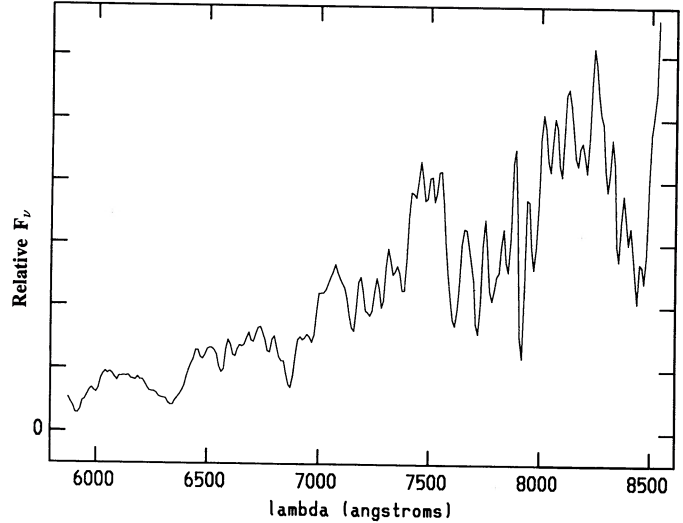


FIG. 6.—NTT spectrum of the companion

ports an extrinsic and contaminating nature of the emission lines at $z = 1.13$ detected in the component (a) spectrum.

Let us summarize the spectral properties of component (a): (1) it has a strong and “red” continuum while the spectral emission lines are likely to be due to the contamination of the neighboring components; (2) its continuum shows striking similarities to the continuum of a field object apparently unrelated with the radio source.

3.2. Spectrum of Component (b): Strong Emission Lines and Faint Reddened Continuum

Component (b) is as bright as component (a) in B , and its spectroscopy reveals strong emission lines plus a faint continuum. Indeed, the bulk of the emission-line activity of the whole optical emission of 3CR 368 appears concentrated in component (b): (1) emission line fluxes of Mg II, [O II] $\lambda 3727$ and [Ne III] $\lambda 3869$ in component (b) dominate those of the other components (see Table 1); (2) Mg II $\lambda 2799$ emission line in component (b)—which has a higher flux than the sum of the flux of all the other components—has a somewhat broad-line profile with a velocity dispersion around 2000 km s^{-1} , while it is a narrow line for all the other components (see Fig. 4b and Table 1); (3) we have also marginally detected a high-ionization line—[Ne V] $\lambda 3426$ —in this component and also at a lower level in component (e). Component (b) continuum appears rather flat with a slight decrease from the red end to the blue end of its spectrum, such a property can be extended from 4500 \AA to $2.2 \mu\text{m}$ from the high resolution broad-band photometry (Le Fèvre et al. 1988a; Djorgovski et al. 1990).

3.3. Similarity between the Spectra of (c) and (e)

Spectra of components (c) and (e) are dominated by the presence of strong emission lines, with no or marginally detected continua in the spectroscopic data, but they do have continuum emission, since they are detected in R and especially in B frames, both broad filters including no or only faint emission lines. It seems reasonable to state that these faint continua are rather flat from B to K ($2.2 \mu\text{m}$) since Chambers et al. (1988) did not detect component (c) in their infrared image, nor did Djorgovski et al. (1990). Strong emission lines are blueshifted by $\sim 550 \text{ km s}^{-1}$ relative to component (b) and are associated with large-velocity regions—up to 1000 km s^{-1} for the [O II]

line—which are also spatially extended. The most striking fact is the intriguing coincidence at less than 100 km s^{-1} between the mean velocities of (c) and (e), which is well below their intrinsic velocity dispersion. Velocity of the $[\text{O II}] \lambda 3727$ gas relative to component (b) emission has two maxima, one on (e), the other on the northern edge of (c), a significant minimum on the southern edge of (c) and a marginal minimum just on the component (a) center (see Fig. 4). The ratio R of the $[\text{O II}] \lambda 3727$ flux to the $\text{Mg II} \lambda 2799$ flux strongly decreases from 28 for component (c) to 9 for component (e). More generally, there is a spatial discrimination which depends on the nature of the emission: blue continuum and the forbidden line $[\text{O II}] \lambda 3727$ are dominant in a region coincident with the southern radio component, while $\text{Mg II} \lambda 2799$ and the possible highly ionized $[\text{Ne V}] \lambda 3426$ are stronger relatively to $[\text{O II}]$ in a region much closer to component (b) (see Figs. 4a and 4b). Red continuum and the $[\text{Ne III}] \lambda 3869$ line seem to come from intermediate regions.

3.4. Global and Significant Observational Features of 3CR 368

Before attempting to interpret such a large amount of data, let us summarize previous results and our new observations in order to define a set of significant observations that any interpretations of 3CR 368 should account for; this includes the following:

1. The multiple-component morphology from UV to IR, with striking spectral discrepancies between the components which suggests different origins (Spinrad 1982; Djorgovski et al. 1987; Chambers et al. 1988; Le Fèvre et al. 1988a; Djorgovski et al. 1990; this paper).
2. The elongation of the whole optical structure which follows within 20° the radio axis (McCarthy et al. 1987; Le Fèvre et al. 1988a); note also the spatial coincidence between optical emission—especially the blue continuum and the $[\text{O II}] \lambda 3727$ emission-line region—and the southern radio component.
3. The high radio spectral index $\alpha = 1.2$ (see, e.g., Spinrad et al. 1985) and the radio polarization (Djorgovski et al. 1987).
4. The coincidence ($\pm 1''$) of (a) with the radio “core” found by Djorgovski et al. (1987), and Chambers et al. (1988), as derived from the astrometry of the field (Kristian et al. 1978).
5. The optical polarization properties recently found by di Serego Alighieri et al. (1989) and confirmed by Scarrott, Rolph, & Tadhunter (1990a), with their spatial distribution.
6. The component (a) spectrum which resembles a continuum spectrum with several added contaminating lines due to neighboring emission; the component (a) SED without emission lines is very similar to the one of a companion object 6"3 south dominated by a sharp “break” at 7300 \AA .
7. The special place taken by the component (b) which is redshifted by $\sim 600 \text{ km s}^{-1}$ from the other components while it appears to be the most active component in the emission lines, with some clues of a nuclear activity.
8. The striking similarity between the (c) and (e) velocities and colors.

In the following sections we will examine several interpretations and compare them to the preceding set of significant observational data. The overall picture of 3CR 368 is dominated by the component (a) on which any interpretation of the optical/IR counterpart properties strongly depends. We will examine several alternatives which could explain the data on component (a) by following an increasing order of probability. Then we will examine the intrinsic properties of 3CR 368 and its true optical counterparts.

4. NATURE OF THE BRIGHT AND RED COMPONENT (a)

4.1. Implausibility for $z = 1.13$

If component (a) was a galaxy, a redshift of 1.133 would not fit the continuum. The observed “break” would correspond to a rest wavelength of 3372 \AA and the other features detected in the continuum would not be fitted at this redshift. It seems very unlikely that such an abrupt “break”—twofold increase of the flux from $\lambda 7250$ to $\lambda 7350$ —could be interpreted as an AGN spectrum extinguished by dust as proposed by Djorgovski et al. (1990). If this was a correct explanation, it would totally extinct the blue continuum which is in contradiction with the data. One could also try to interpret the component (a) spectrum by a bimodal model of a hot plus cold stellar component and reproduce the 7300 \AA “break” by adjusting the weight of the two stellar populations. However, the resemblance of (a) with the companion, a faint object apparently unrelated to the radio source, added to the fact that emission lines at $z = 1.13$ detected for (a) can be explained by contamination from the emission of its close neighbors (c) and (e) led us to investigate the possibility that component (a) is an unrelated foreground object falling on the line of sight of the true optical counterpart of 3CR 368.

4.2. A Foreground gE at $z = 0.85$?

We originally believed that component (a) was a foreground galaxy. The 7300 \AA “break” added to the similarity between the component (a) and companion spectra were advocating $z = 0.85$ for both objects and the increase of the flux around 8000 \AA was also well fitted. If component (a) is a galaxy at $z = 0.85$, it would be a giant elliptical or even a cD galaxy— $M_R \sim -23$ —most of its strong luminosity being provided by old stars emission, while at least part of the blue emission would be due to the contamination from (c) and (e) continuum. Such an explanation was also consistent with the fact that blueward of 7000 \AA the continuum had been found spatially extended, $1''.2$ FWHM, while redward of 7300 \AA it appeared hardly or not spatially resolved, i.e., $0''.5$ FWHM (FWHMs corrected from instrumental effects). It might also have been due to a discrimination of the stellar spatial distribution with red and old stars concentrated inside the galaxy center, with blue and young stars at the outer part of the galaxy. Stellar appearance of the red continuum, as well as the companion itself, may have been explained by the surface brightness dimming, 2.7 mag at $z = 0.85$. Indeed a bright elliptical with $r_{\text{eff}} = 10 \text{ kpc}$ would be hardly spatially resolved on our spectroscopic frames down to $27 \text{ mag arcsec}^{-2}$ in R (see Fig. 3 of Hammer 1989).

We have also investigated the gravitational lensing properties caused by the superposition of a galaxy at $z = 0.85$ just on an extended source at $z = 1.13$. We have modeled it following the numerical procedures which were described by Hammer & Rigaut (1989). If component (a) was at $z = 0.85$, both (e) and the radio “core” (Djorgovski et al. 1987; Chambers et al. 1988) should be the secondary gravitational images of (c) and of the northern part of the southern radio component, respectively. A relatively low M/L ratio of 10 inside a disk of 10 kpc radius around the lens center was needed for the component (a) to gravitationally split background extended sources at $z = 1.133$ and account for the separation between the assumed multiple images. Such a scenario reproduces the (c) and (e) spectroscopic similarities as well as the radio data. Component (a) at $z = 0.85$ would provide moderate gravitational magnifications of the extended background sources—less than a half-

magnitude—but the luminosity of the whole object was especially affected by the removing of the lens itself.

However, the “bump” at 7026 Å and the decrease of the flux between 7600 Å and 7800 Å were not well understood and led us to investigate the following possibility.

4.3. A Faint Galactic Cool Star?

4.3.1. Arguments for a M5 star

The best fit to the component (a) spectrum is provided by a nonredshifted stellar spectrum (Hammer, Le Fèvre, & Proust 1990). We identify the slope changes of the continuum as due to strong and large absorptions bands of TiO which characterize M cool star spectra. All the continuum features reported in § 3.1 are reproduced. Moreover, although the calibration of our CFHT spectrum for $\lambda \geq 8500$ Å is not excellent, the continuum peaks at ~ 8800 Å as expected and seems also to be detected up to ~ 9250 Å (Fig. 2). Measurements of the absorption strengths of TiO at 7050 Å and between 7500 and 7700 Å are comparable to those of M4–M5 stars. To minimize contamination problems, we have used $R-K$ rather than $B-R$ indices, assuming $K = 17.5$ (Djorgovski et al. 1990). We derive $R-K = 4$, an usual value for M5 stars (Wing 1983). The combination of these arguments lead us to conclude that component (a) is a faint ($R = 21.5$) M4.5 or M5 star. Some other features—blend of K I $\lambda 7665$, $\lambda 7699$ and blend Na I $\lambda 8193$ and $\lambda 8195$ Å absorptions—are also barely visible on the spectrum (see Figs. 7a and 7b). Figures 7a and 7b show the superposition of component (c) and the dwarf M4.5 star Rox 127 spectra (J. Bouvier, private communication) with a scaling of the flux of Rox 127 to equal the flux of component (a) between 7100 and 7600 Å, which reproduces all the significant features of component (a). This provides the best possible estimate of the magnitude and colour of the star, $R = 21.5$ and $B-R = 2.7$. 3CR 368 lies in a region of very high stellar density not very far from the direction of the Galactic center. The likelihood of such a superposition can be estimated from observed star counts at faint magnitudes. A rough prediction is provided by the model of Bahcall & Soneira (1980). An extrapolation of

their results from $b = 20^\circ$ to $b = 15^\circ$ and for $l = 38^\circ$ yield about 69,200 stars per square degree having a magnitude up to $B = 24$ which could be compared with more than 80 similar stars we found in our 130×170 arcsec² B frame, i.e., $\sim 47,000$ stars per square degree. A similar density of stars is found on our field for $R = 22$ and is ~ 5 times the density of galaxies as derived from counts of galaxies (Tyson 1988). The probability that such a star is seen in projection within a ~ 15 arcsec² surface—the size of 3CR 368 optical counterpart at $z = 1.13$ —reaches 6%. The projection of faint stars on the high- z 3CR lines of sight is then not unlikely knowing that there are several tens of 3CR extragalactic sources having $10^\circ \leq b \leq 20^\circ$. Since 66% of the total number of stars in our Galaxy are M dwarf stars (see, e.g., Allen 1973), it is not surprising—*a posteriori*—that they contaminate some extragalactic extended sources. One may also note the “close encounters” of (bright) Galactic stars on other high- z 3CR galaxies such as 3C 230 ($z = 1.487$, Hammer & Le Fèvre 1990), and 3C 294 ($z = 1.78$).

4.3.2. Main Properties of Component (a) as a Dwarf Star

In order to elucidate the properties of 3CR 368 at $z = 1.13$, it is crucial to learn more about the properties of the contaminating M star before removing it. It seems likely that component (a) is an M dwarf star, since M dwarf stars are 3×10^5 more numerous than M giant stars and should dominate counts at faint magnitudes (Dawson 1981; Mikami & Ishida 1981). Our spectroscopy seems also to support the M dwarf hypothesis since the Ca H bands are detected. Assuming that component (a) is an M dwarf of type between 4.5 and 5.5, let us estimate its general properties from the empirical relations presented by Rodonò (1986). From $R-K = 4$, we derived an absolute bolometric magnitude $M_{\text{bol}} = 11.8$ which is typical for a low-mass $M/M_\odot = 0.1$ and cold $T_{\text{eff}} = 3000$ K star. Its estimated distance would be 0.5 kpc, with a factor of 2 of uncertainty, and it probably belongs to the Galactic disk. The angular velocity of the star relative to the extragalactic line of sight is $W \sim 0''.04 (V/100 \text{ km s}^{-1}) (500 \text{ pc}^{-1} D)$ per year, where V is the velocity of the star relatively to the 3CR 368 line of

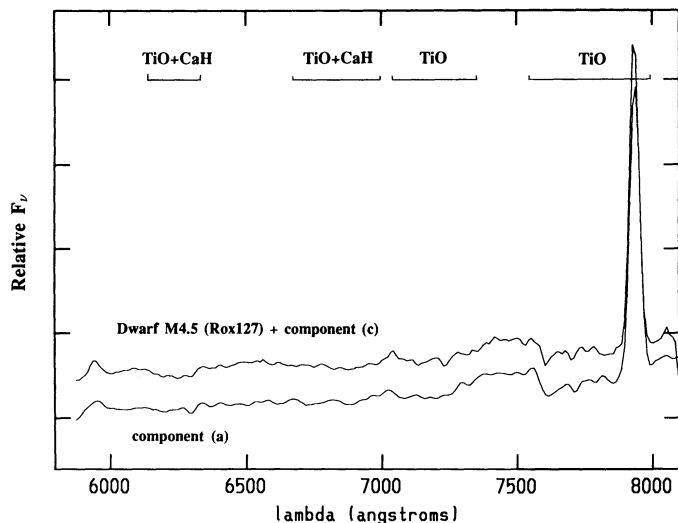


FIG. 7a

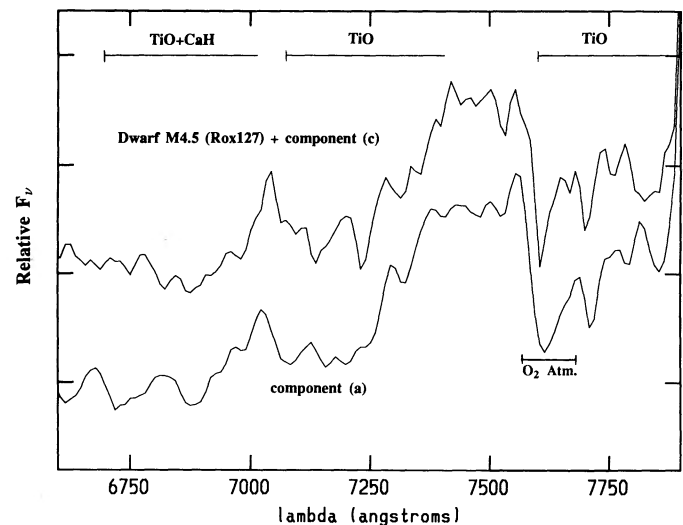


FIG. 7b

FIG. 7.—NTT spectrum of (a) compared to the sum of the NTT spectrum of (c) and of the scaled spectrum of the dwarf M4.5 Galactic star Rox 127: (a) 5800–8100 Å range; (b) 6600–7900 Å enlargement.

sight, and D is its actual distance to us. The cool star spectral type of component (a) favors that it is an emission-line star since the fraction of dMe stars among all M dwarfs increases with advancing spectral subclass to nearly 100% for M5 (Joy & Abt 1974). Only a marginal $H\alpha$ line is found at 6563 Å blended with the continuum “bump” expected around this wavelength. This is not conclusive since low-resolution spectroscopy should dilute a 1 Å FWHM emission line under our spectral resolution of 38 Å.

4.3.3. *To What Extent Are Properties of 3CR 368 Due to the Contaminating Star?*

Let us now assume that component (a) is a dMe star and try to estimate how and to what extent it could be responsible for observational features previously found and assumed to be due to the $z = 1.13$ background source. Dwarf active stars are all flare stars, and they may be young objects or old members of binary systems (Rodonò 1986). They have X-ray emission and at least the most active of them also present radio emission with $L_R = 10^{13}$ to 10^{15} ergs s^{-1} Hz^{-1} . Their emissions at all wavelengths present variations up to several tenths of magnitudes occurring on time scales from less than 1 s to 10 minutes (flares) and from months to years (long-term variability). If the star lay at 0.5 kpc, the corresponding radio flux could reach several mJy at 6 cm, and it could still have been observed by Djorgovski et al. (1987) and by Chambers et al. (1988) as the unresolved radio “core” they found at the location of component (a) (within the astrometric uncertainties). Moreover its ~ 3 mJy radio flux measured by the later group exceeds by several times the 0.45 mJy flux found by Djorgovski et al. (1987) at 6 cm. This could be due to an intrinsic variability and be linked with a very active star, unless measurement errors were larger than expected. Another intriguing fact comes from the comparison of the two K ($2.2 \mu m$) maps first published by Chambers et al. (1988) and more recently by Djorgovski et al. (1990). The former group found two blobs having about similar fluxes, while the later have resolved the blob corresponding to component (a) into two subcomponents which obviously strongly dominates the infrared emission of the whole object. Moreover, the enigmatic infrared component—called K by Djorgovski et al. (1990)—which is detected only at $2.2 \mu m$ should be interpreted carefully. It lies between components (e) and (b) at a location where the visual continuum (B and R filter) and the emission lines [$O II$] $\lambda 3727$ and $Mg II$ $\lambda 2799$ present sharp minima. If it is real, its SED presents a dramatic increase between 1.65 and $2.2 \mu m$. This might be due to complex mechanisms like dust obscuration if it was interpreted with a $z = 1.13$ source, but it also may be a galactic star cooler than component (a). In this later case, both objects would likely belong to a common binary system with a projected axis of 600 AU.

Optical polarization measurements (di Seregho Alighieri et al. 1989; Scarrott et al. 1990b) have revealed strong polarization with a wavelength dependency consistent with an interstellar origin. The first authors had rejected an interstellar interpretation of their results because they found no polarization for various objects lying in the 3CR 368 field. However, the fact that the extragalactic source falls just behind a Galactic active star requires a reinvestigation of the optical polarization origin. Unfortunately, polarization properties of stars are mostly coming from studies of well-documented bright stars—Miras and giant and supergiant semiregulars (see, e.g., Querci 1986). Polarization properties seem to be linked with the emission-line activity (Shawl 1974) and to be especially fre-

quent for spectral type later than M4 (Dyck & Jennings 1974). To our knowledge there is no observational evidence for or against polarization of the optical light from dMe stars. However, several observational features favor a link with the component (a) if it is a dMe star:

1. The polarization values and their wavelength dependencies found by di Seregho Alighieri et al. (1989) are consistent with the polarization properties of red variable stars (Querci 1986).

2. Scarrott et al. (1990a) have published high spatial resolution maps of the 3CR 368 optical polarization for which the northern as well as southern extensions “exhibit a centrosymmetric polarization pattern centered on the bright nucleus,” i.e., the component (a). This map strikingly resembles the map of the galactic bipolar nebulae associated with IRAS 07131–0147 (Scarrott et al. 1990b).

3. The faint component (d) is seen optically polarized (Scarrott et al. 1990a) while it is likely to be also foreground since [$O II$] $\lambda 3727$ at $z = 1.13$ has not been detected (Djorgovski et al. 1987).

On the other hand, there are several difficulties to assume that the polarization of the whole 3CR 368 optical counterpart is only due to a stellar origin linked with component (a). The radius of the circumstellar dust region should reach about 2×10^{16} cm which is quite large. The polarization of the red light slightly decreases through the peak emission of the star. There is a good coincidence between the polarization angle of the component (b) and the line perpendicular to the radio axis. To understand these intriguing properties better, new polarimetric observations of both other dMe stars and other distant radio galaxies are needed.

Let us finally examine the extreme hypothesis that the whole radio emission is due to the foreground star. Indeed there are some stellar sources which resembles classic FR II extragalactic radio sources. If we were observing Sco X-1 just in front of a background galaxy, it would present a radio flux and morphology similar to 3CR 368 except that the central radio component would be more luminous. Such an hypothesis appears unlikely since (1) it does not account for the spatial coincidence of the extragalactic component (c) with the southern radio lobe; and (2) the superposition of a $B = 23$ galaxy within a few arcseconds from a strong stellar radio source is associated with a probability lower than some 0.1%.

Summarizing, the presence of a cool Galactic star highly complicates the interpretation of 3CR 368, which is by far the most observed high-redshift galaxy at all wavelengths. Removing of the star leads to the following:

1. A dramatic change in the morphology of the background object;

2. A decrease of the luminosity of the source especially at red and IR wavelengths and a dramatic change of its spectral energy distribution; and

3. A possible stellar origin for the additional component K detected by Djorgovski et al. (1990), the radio core detected at 6 cm, and the polarization properties.

This also leads us to reassess the true intrinsic properties of the background source.

5. NATURE OF THE BACKGROUND SOURCE AT $z = 1.13$

5.1. *Global Properties after Removing Component (a)*

Whatever is the exact nature of the component (a), it should be removed to reveal the intrinsic nature of 3CR 368, because it is foreground. The faint component (d) (see Le Fèvre et al.

TABLE 2

MAGNITUDES B, R, AND K FOR 3C 368 BEFORE AND AFTER CORRECTION FROM THE CONTAMINATION OF COMPONENT (a)

Magnitude	Before Correction	After Correction
B	21.46	21.63
R	20.22	20.85
K (7".4 aperture)	16.8	≥ 17.8

1988) should be also removed because it is believed to be foreground since $[\text{O II}] \lambda 3727$ at $z = 1.13$ has not been detected (Djorgovski et al. 1987). We removed components (a) and (d) from our *B* and *R* images using a PSF carefully built from field stars; Table 2 summarizes the corrected broad-band magnitudes compared to the former measurements. The resulting *K* magnitude could not be accurately estimated especially because the infrared measurements vary from one author to another from $K = 16.68$ through a 7".4 aperture (Lilly & Longair 1984) to $K = 17.07$ through a 7" aperture (Eisenhardt & Lebofsky 1987). New infrared imaging has been recently obtained by Djorgovski et al. (1990) who have estimated $K = 17.5$ for the single component (a) and found $K = 16.8$ through a 7".4 aperture (S. Djorgovski, private communication). On a similar aperture we have carefully measured $R = 20.05$, and $R = 20.56$ for the residual emission after subtraction of components (a) and (d). Removing the $R-K = 4$ star from this aperture then provides the color index of the residual emission, $R-K = 2.77$. It is likely to be the color index of the residual 3CR 368 at $z = 1.13$, which then should have $K = 17.8$. Moreover one would expect a higher value if the components (K) and (R) of Djorgovski et al. (1990) are also foreground. Therefore the spectral energy distribution of the whole background source is considerably flatter than previously believed (Lilly 1989; Chambers & Charlot 1990); Figure 8 shows the new SED corrected for the dwarf M4.5 star contamination compared to the uncorrected SED. This source shows no evidence for a "red bump" as invoked by Lilly (1989) and Miley & Chambers (1989) to be a common property of high-redshift radio galaxies (Fig. 8). This also means that after removing contaminating foreground objects, 3CR 368 lies at least 1 mag above the $K-z$ relation established by Lilly & Longair (1984).

Radio properties are only slightly affected by removing of the foreground component (a). Astrometry of the field from the Kristian et al. (1978) data locates the radio core between components (a) and (e) with better than 1" accuracy. The radio core should be removed if component (a) is an active radio-emitting star or if it was a foreground lensing elliptical galaxy. If this is true, component (b) is the closest optical object to the radio centroid and then the likeliest optical counterpart. Component (b) is not affected by the removing of the foreground object, while the similarity between the (c) and (e) spectra strongly favors that they belong to the same large and elongated $4'' \times 2''$ diffuse region. The resulting morphological appearance of the optical emission is an association of a relatively compact but not stellar object with a diffuse and elongated emission line region which extends over 45×20 kpc and appears associated with the southern radio component. Figure 9 shows the appearance of the 3C 368 source in *R* before and after removal of a stellar profile of the same magnitude as (a), at the location of (a), as well as a removal of (d) also believed to be foreground.

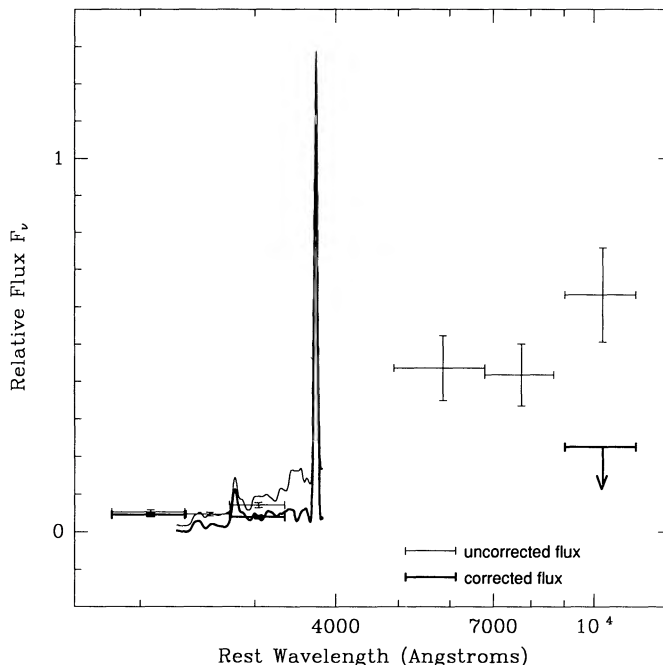


FIG. 8.—Spectral energy distribution of 3C 368 before and after correction by the M4.5 dwarf star. Uncorrected flux has been taken from the broad data of Chambers & Charlot (1990) and Table 2 of the present paper, combined with our total CFHT spectrum. The flux has been corrected as described in the text for the broad-band data. The corrected spectrum of the whole 3CR 368 has been obtained after subtraction of the dwarf M4.5 star Rox 127 spectrum which was adjusted for best fit on the continuum of component (a).

Let us now examine the detailed properties of the $z = 1.13$ source.

5.2. Properties of Component (b): An Active Galactic Nucleus

Component (b) presents the highest emission-line activity of the whole object with velocity dispersions reaching 2000 km s^{-1} for the $\text{Mg II } \lambda 2799$ emission and about 1000 km s^{-1} for the $[\text{O II}] \lambda 3727$ emission. This emission-line activity appears to belong to quite compact regions which are not really spatially resolved in our spectroscopic frames (Fig. 4). We therefore think that the spectroscopy of compact (b) reveals the presence of an active galactic nucleus with a prominent narrow-line region and with some indication of a presence of a broad-line region.

Component (b) shows an elongated structure in our *R* frame (Le Fèvre et al. 1988) which could recall elliptical galaxy shapes. The velocity of the $[\text{O II}]$ emission gas along this structure is compatible with an underprojected (not deprojected) rotational velocity—half the difference in the average velocities of the gas on opposite sides of the nucleus—reaching 330 km s^{-1} over $2''.6$ or 30 kpc which is a much larger value than the rotational velocities of a typical elliptical stellar system. Its spectroscopy reveals a faint continuum which is compatible with a power-law continuum possibly reddened by dust extinction rather than with the spectrum of an elliptical galaxy redshifted at $z = 1.133$, since we found no evidence for a 4000 \AA break around 8500 \AA . Within our detection limits, there is no direct or indirect evidence for stellar emission in component (b).

Indeed, infrared and visual imaging and photometry suggest that the component (b) continuum is flat or slightly reddened from 2000 to 10000 \AA at rest (Fig. 8). Since the reddening is

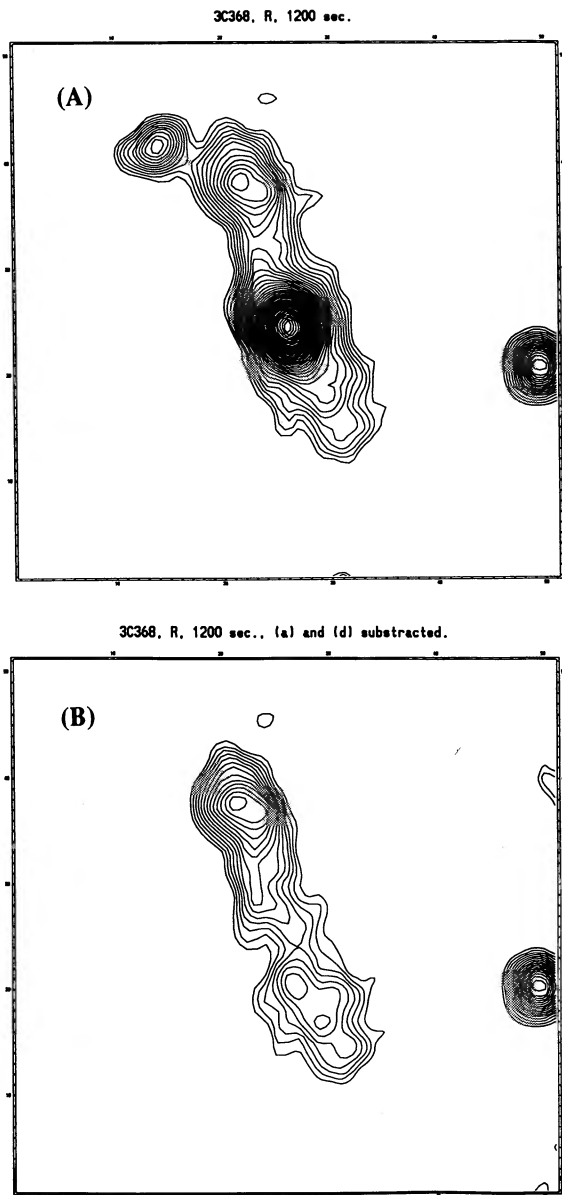


FIG. 9.—R image of 3C 368 before (a) and after (b) correcting from the contamination of components (a) and (d) by subtracting stellar images of same magnitudes at the (a) and (d) locations.

probably associated with the polarization properties, whatever are their origins, we believe that component (b)—and also component (c)—is even bluer than $B-R = 1.12$. Component (b) continuum could be fitted by a single power law from IR to UV plus an excess of emission around 2000 \AA at rest—the UV “bump”—which is a characteristic of most of the QSOs (see Fig. 8).

5.3. 3CR 368: An AGN with an Extended and Blueshifted Emission-Line Region

Emission-line activity, spectral energy distribution of the continuum, and radio/optical astrometry favor that component (b) is the central engine—the AGN—which supplies the emission of the whole object. Blueshifted by about 550 km s^{-1} , there is a blue and diffuse emission-line region (EELR)—

components (c) and (e)—which extends over 45 kpc. Preliminary results indicate that these properties are shared by other high- z 3CR galaxies, including 3CR 238 (F. Hammer & O. Le Fèvre, in preparation). Highly ionized gas and Mg II emission-line regions appear less extended and closer to the AGN than the continuum and the lower ionized gas ([Ne III] $\lambda 3869$, [O II] $\lambda 3727$). Blue continuum and [O II] emission-line regions strikingly coincide with the southern radio component which present a jet plus lobe structure. The velocity field along the [O II] EELR is compatible with a slowing down of the gas relative to the AGN, i.e., 550 km s^{-1} close to component (b) against 200 km s^{-1} at the southern edge of component (c). There are also extremely large velocity gradients up to 1500 km s^{-1} along the slit. A careful comparison between our CFHT and NTT spectroscopy at two different slit locations provides also a velocity difference of roughly 400 km s^{-1} between the line passing through the central parts of the EELR and its eastern edge. The component (c) spectroscopy from CFHT shows a rather large [O II] line width of $\sim 1800 \text{ km s}^{-1}$ —while spectroscopy from the NTT does not even resolve it (Fig. 5c). This may be compared with the spectroscopy of Djorgovski et al. (1987) which found an intermediate result—width $\sim 800 \text{ km s}^{-1}$; it is probable that their slit was oriented at an angular position between our NTT and CFHT slit angular positions. It implies that large velocity gradients are due to the whole three-dimensional extent of the EELR and suggests a conelike morphology.

There is a striking similarity between the whole spectrum of the EELR and the AGN spectrum. This property is already shared by most of the low- z radio galaxies (see, e.g., Robinson 1989) which show similarities between EELR and nuclear narrow-line regions. Moreover, the broad-band color indices of the EELR are similar to those of the AGN although the surface brightness of the continuum associated with the EELR is fainter and undetected by our spectroscopy. Other intriguing properties are the facts that the Mg II EELR is less extended and closer to the AGN than the other EELR and that it is also blue shifted relatively to [O II] and [Ne III] EELR as in the AGN. Roughly speaking and down to our spatial resolution, the EELR structure of 3CR 368 may resemble the inner parts of an AGN but scaled up in an anisotropic way. This may suggest that the EELR is photoionized by the AGN continuum source. However, one has to account for the fact that the total energy from the EELR exceeds the one of the AGN both in [O II] $\lambda 3727$ and in continuum.

Several scenarios have been proposed to explain 3CR high- z galaxies and especially their EELR morphologies and continua. Among them the most popular are the triggering of star formation by radio jets (McCarthy et al. 1987; Daly 1990) and the highly collimated beams scattered by dust or electrons (Tadhunter, Fosbury, & di Seregho Alighieri 1989; Fabian 1989). It is crucial to determine what is stellar and what is linked with the AGN in these sources. The AGN is responsible for the radio power which strongly dominates the energy emission at all wavelengths. The starburst scenario has succeeded in reproducing strong emission lines but failed to explain the tightness of the $K-z$ diagram (Bithell & Rees 1990). They are also associated with large velocity gradients—up to 2000 km s^{-1} (this paper; F. Hammer & O. Le Fèvre, in preparation)—which is difficult to reconcile with a stellar origin. Similarities between these emission lines and the narrow emission lines found in active nuclei plead for a close link between emission lines and the AGN. 3CR 368 presents a very good coincidence

between [O II] EELR and visual continuum (Djorgovski et al. 1987). We believe that a stellar origin is questionable, at least for this part of the continuum which is so well aligned with the radio axis. 3CR 368 presents a slightly reddened continuum which flattens at its blue end (Fig. 8). We did not find the 4000 Å break which would be detected at 8500 Å if the continuum was of stellar origin. On the other hand, the SED could be fitted by a power law and the still slightly red continuum might be due to the Balmer continuum. The origin of the reddest part of the continuum is still unclear since Djorgovski et al. (1990) have found alignments between radio and infrared. This seems to reject for this source the scenario of an old star population as proposed by Lilly (1989). Note that it was proposed in order to explain the tightness of the K - z relationship, while the corrected 3CR 368 lies at least 2.5σ above the mean relation. Our main result for the residual 3CR 368 at $z = 1.13$ is that it could be a new example of an AGN with an EELR linked with its radio activity, while there are no evidences of stellar activity.

6. CONCLUSION

Thanks to our high spatial resolution spectroscopy we have discovered that the multicomponent 3CR 368 source is indeed strongly contaminated by a foreground object. The foreground bright object has a strong red continuum while the remaining objects at $z = 1.133$ have blue flat and faint continua dominated by strong emission lines. The foreground object is found likely to be a M4.5–5 Galactic star from its spectrum and strongly alters the known properties of 3CR 368. The SED of 3CR 368 was previously believed to have a “red bump” which was commonly interpreted as dominated by a combination of various stellar populations at $z = 1.13$. Removing the bright foreground star allows a more accurate view of the intrinsic properties of 3CR 368 at $z = 1.13$. The SED is deeply modified (see Fig. 8): the infrared magnitudes are fainter by as much as a magnitude or more; the “red bump” was of stellar origin but from a $z = 0$ star! The remaining object at $z = 1.13$ is likely to be an AGN with a very large and blueshifted emission line region having a cone-like morphology and probably associated with the radio emission. There is no clear evidence for stellar emission and conversely several hints of nuclear activity and even for the presence of a hidden QSO have been presented. It might then appear irrelevant to classify 3CR 368 as a galaxy.

We have previously predicted that the high- z 3CR galaxies were likely to be contaminated by foreground galaxies due to selection effects (Hammer et al. 1986). This idea originally came from the extremely high luminosities required for these sources assumed to be galaxies, and from their extremely low density—less than one per (1000 Mpc)³—which suggested strong selection effects. The later could be due either to intrinsic peculiar properties of the source—“powerful monster”—or to gravita-

tional magnification of their (radio) luminosities which allow some less powerful and more numerous high- z radio sources to enter the 3CR catalog. The signature of the later mechanism should be an excess of foreground galaxies close to the source lines of sight, and we have some evidences that such an excess does exist (Hammer & Le Fèvre 1990). 3CR 368 is still more peculiar than we had imagined since it is a “powerful monster” both from its radio power and from its contamination by a Galactic star. At the low Galactic latitude, $b = 15^\circ$, of 3CR 368, the contamination by stars is about 5 times more probable than the contamination by foreground galaxies down to $R = 22$. This strengthens *a posteriori* the idea that the severe selection criterion made the high- z 3CR galaxies anomalous objects. After removing the foreground object, 3CR 368 can be described by an AGN plus an extended emission region while previously it appeared as a five-component galaxy dominated by stellar activity. The brightness of 3CR 368 at $z = 1.13$ has to be lowered by 0.5 mag to more than 1 mag from optical to IR wavelengths. The results on 3CR 368 provide us a new occasion to notice at which point it might be irrelevant to derive evolution and/or cosmological parameters from powerful radio galaxies (see Djorgovski, Spinrad, & Marr 1985; Rocca-Volmerange & Guiderdoni 1987; Chambers & Charlot 1990) which are dominated by their radio power and likely contaminated by foreground stars or galaxies. The heterogeneous nature of their components also pleads against attempts to derive photometric redshifts from them as it was done by Dunlop et al. (1988), and one is warned about the interpretation of the multiple-component morphology of these sources (see Hammer 1989) without paying attention to the contamination by foreground objects as is the case for 3CR 368. Finally, the results on the properties of the real 3C 368 at $z = 1.13$ may also prove to extend to other high-redshift radio galaxies: preliminary results show that some of the 3CR high- z galaxies exhibit a structure similar to 3CR 368; i.e., an AGN combined with a one-sided EELR. They may be a new class of extragalactic sources for which alignments between the radio and optical emissions are related to their extremely high radio power.

We thank N. Arimoto, J. Bouvier, S. di Seregho Alighieri, G. Djorgovski, D. Gillet, M. Joly, S. Lilly, M. Mouchet, V. Petrosian, A. Stockton, and C. Tadhunter for useful discussions, suggestions, and/or private communications. Special thanks to C. Boisson for her advice and careful reading of the manuscript. We are also grateful to the referee, P. Eisenhardt, for similar reasons. Part of the observations were obtained within the framework of the ESO key program on gravitational lensing, and we thank ESO and J. Surdej for their allocation of time. We finally thank the CFHT and ESO night assistants for their skillful help in acquiring the data as well as R. McLaren for his help during the NTT run.

REFERENCES

- Allen, C. W. 1973, *Astrophysical Quantities* (London: Athlone)
 Bahcall, J. N., & Soneira, R. M. 1980, *ApJS*, 44, 73
 Bithell, M., & Rees, M. J. 1990, *MNRAS*, 242, 570
 Chambers, K. C., & Charlot, S. 1990, *ApJ*, 348, L1
 Chambers, K. C., Miley, G. K., & Joyce, R. R. 1988, *ApJ*, 329, L75
 Chambers, K. C., Miley, G. K., & van Breugel, W. 1987, *Nature*, 329, 604
 Daly, R. A. 1990, *ApJ*, 355, 416
 Dawson, P. C. 1981, *AJ*, 86, 1200
 di Seregho Alighieri, S., Fosbury, R., Quinn, P., & Tadhunter, C. 1989, *Nature*, 341, 307
 Djorgovski, S., Spinrad, H., & Marr, J. 1985, in *New Aspects of Galaxy Photometry*, ed. J. L. Nieto (New York: Springer), p. 193
 Djorgovski, S., Spinrad, H., Pedelty, J. A., Rudnick, L., & Stockton, A. 1987, *AJ*, 93, 1307
 Djorgovski, S., Weir, N., Matthews, K., & Graham, J. R. 1990, in *Astrophysics with Infrared Arrays*, ed. R. Elston (ASP Conf. Ser.), in press
 Dunlop, J. S., Guiderdoni, B., Rocca-Volmerange, B., Peacock, J. A., & Longair, M. S. 1989, *MNRAS*, 240, 257
 Dyck, H. M., & Jennings, M. C. 1974, *AJ*, 76, 431
 Eisenhardt, P. R., & Chokshi, A. 1990, *ApJ*, 351, L9
 Eisenhardt, P. R., & Lebofsky, M. J. 1987, *ApJ*, 316, 70
 Fabian, A. C. 1989, *MNRAS*, 238, 41P
 Hammer, F. 1989, in *Morphology of High Redshift Galaxies*, 11th European Meeting of IAU (Cambridge: Cambridge University Press), in press

- Hammer, F., & Le Fèvre, O. 1990, *ApJ*, 357, 38
 Hammer, F., Le Fèvre, O., & Proust, D. 1990, *IAU Circ.*, No. 5011
 Hammer, F., Nottale, L., & Le Fèvre, O. 1986, *A&A*, 169, L1
 Hammer, F., & Rigaut, F. 1989, *A&A*, 226, 45
 Joy, A. H., & Abt, H. A. 1974, *ApJS*, 28, 1
 Kristian, J., Sandage, A., & Katem, B. 1978, *ApJ*, 219, 803
 Le Fèvre, O., & Hammer, F. 1988, *ApJ*, 333, L37
 ———. 1990, *ApJ*, 350, L1
 Le Fèvre, O., Hammer, F., & Jones, J. 1988a, *ApJ*, 331, L73
 Le Fèvre, O., Hammer, F., Nottale, L., & Mazure, A. 1988b, *ApJ*, 324, L1
 Lilly, S. J., & Longair, M. S. 1984, *MNRAS*, 211, 833
 Lilly, S. J. 1988, *ApJ*, 333, 161
 ———. 1989, *ApJ*, 340, 77
 ———. 1990, in *The Evolution of the Universe of Galaxies: The Edwin Hubble Symposium*, ed. R. P. Kron (*ASP Conf. Ser.*, 10), in press
 McCarthy, P. J., van Breugel, W., Spinrad, H., & Djorgovski, S. 1987, *ApJ*, 321, L29
 Mikami, T., & Ishida, K., 1981, *PASJ*, 33, 135
 Miley, G., & Chambers, K. 1989, in *ESO Workshop 32 on Extranuclear Activity in Galaxies*, ed. J. A. Meurs & R. A. E. Fosbury (Garching: ESO), p. 259
 Querci, M. 1986, in *The M Type Stars*, ed. H. R. Johnson & F. R. Querci (NASA SP-492), p. 113
 Robinson, A. 1989, in *ESO Workshop 32 on Extranuclear Activity in Galaxies*, ed. J. A. Meurs & R. A. E. Fosbury (Garching: ESO), p. 43
 Rocca-Volmerange, B., & Guiderdoni, B. 1987, in *High Redshift and Primeval Galaxies*, ed. J. Bergeron et al. (Gif-sur-Yvette: Editions Frontières), p. 239
 Rodonò, M. 1986, in *The M Type Stars*, ed. H. R. Johnson & F. R. Querci (NASA SP-492), p. 409
 Scarrott, S., Rolph, C., & Tadhunter, C. 1990a, *MNRAS*, 243, 5P
 Scarrott, S., Rolph, C., Wolstencroft, R., Walker, H., & Sekguchi, K. 1990b, preprint
 Shawl, S. J. 1974, in *Planets, Stars and Nebulae Studied with Photopolarimetry*, ed. T. Gehrels (Tucson: University of Arizona Press), p. 821
 Spinrad, H. 1982, *PASP*, 94, 397
 Spinrad, H., Djorgovski, S., Marr, J., & Aguilar, L. 1985, *PASP*, 97, 932
 Stone, R. P. S. 1977, *ApJ*, 218, 767
 Stone, R. P. S., & Baldwin, J. A. 1983, *MNRAS*, 204, 347
 Tadhunter, C. N., Fosbury, R. A., & di Seregho Alighieri, S. 1989, in *Proc. Como Workshop on BL Lac Objects*, ed. L. Marashi, T. Maccacaro, & M. H. Ulrich (Berlin: Springer), p. 79
 Tyson, N. D. 1988, *AJ*, 96, 1
 Wing, R. F. 1983, in *IAU Colloquium 71, Activity in Red Dwarf Stars*, ed. P. B. Byrne & M. Rodonò (Dordrecht: Reidel), p. 35